crystals

MDPI

Article

Effect of High Temperature Treatment on the Photoluminescence of InGaN Multiple Quantum Wells

Yachen Wang [1,2], Feng Liang [1,*], Degang Zhao [1,3,*], Yuhao Ben [1,2], Jing Yang [1], Zongshun Liu [1] and Ping Chen [1]

[1] State Key Laboratory of Integrated Optoelectronics, Institute of Semiconductors, Chinese Academy of Sciences, Beijing 100083, China; wangyachen21@mails.ucas.ac.cn (Y.W.); yhben@semi.ac.cn (Y.B.); yangjing333@semi.ac.cn (J.Y.); zsliu@semi.ac.cn (Z.L.); pchen@semi.ac.cn (P.C.)
[2] College of Materials Science and Opto-Electronic Technology, University of Chinese Academy of Sciences, Beijing 100049, China
[3] School of Electronic, Electrical and Communication Engineering, University of Chinese Academy of Sciences, Beijing 100049, China
* Correspondence: liangfeng13@semi.ac.cn (F.L.); dgzhao@red.semi.ac.cn (D.Z.)

Abstract: In this work, the photoluminescence (PL) properties of three as-grown InGaN/GaN multiple quantum well (MQW) structures which are heat-treated under different temperatures with nitrogen (N_2) atmosphere are investigated. Temperature-dependent photoluminescence (PL) analysis was used to characterize the depth of localized states and defect density formed in MQWs. By fitting the positions of luminescence peaks with an LSE model, we find that deeper localized states are formed in the MQWs after high-temperature treatment. The experimental results show that the luminescence intensity of the sample heat-treated at 880 °C is significantly improved, which may be due to the shielding effect of In clusters on defects. While the luminescence efficiency decreases because of the higher defect density caused by the decomposition of the InGaN QW layer when the sample is heat-treated at 1020 °C. Moreover, the atomic force microscope results show that the increase in heat-treatment temperature leads to an increase in the width of surface steps due to the rearrangement of surface atoms in a high-temperature environment.

Keywords: InGaN quantum well; photoluminescence; localized states; high-temperature treatment

Citation: Wang, Y.; Liang, F.; Zhao, D.; Ben, Y.; Yang, J.; Liu, Z.; Chen, P. Effect of High Temperature Treatment on the Photoluminescence of InGaN Multiple Quantum Wells. *Crystals* **2022**, *12*, 839. https://doi.org/10.3390/cryst12060839

Academic Editor: M. Ajmal Khan

Received: 10 May 2022
Accepted: 13 June 2022
Published: 14 June 2022

Publisher's Note: MDPI stays neutral with regard to jurisdictional claims in published maps and institutional affiliations.

Copyright: © 2022 by the authors. Licensee MDPI, Basel, Switzerland. This article is an open access article distributed under the terms and conditions of the Creative Commons Attribution (CC BY) license (https://creativecommons.org/licenses/by/4.0/).

1. Introduction

GaN and other III-nitrides, considered as the third generation of semiconductor materials, are widely used in many fields such as light storage, illumination, display, and detection [1–3]. Recently, Liang et al. [4] reported the room-temperature continuous-wave operation of 6.0 W GaN-based blue laser diode (LD) with an emission wavelength at around 442 nm. In GaN-based blue LDs, InGaN/GaN multi-quantum wells (MQWs) are widely used as active regions and their crystal quality will significantly affect the luminescence quality [5–7] and then the laser performance [8]. Scientists have made great efforts to grow InGaN/GaN materials with low defect density and high interface uniformity [9,10]. However, due to the large lattice mismatch and severe polarization effect between the two compounds of GaN and InN [11], high-quality InGaN/GaN heterogeneous materials still need to be studied. Another problem for the epitaxial growth of InGaN is how to improve the incorporation efficiency of In atoms into the InGaN quantum well (QW) layers. Due to the low decomposition temperature of InN at about 600 °C [12] and the immiscibility gap between InN and GaN [13], it is necessary for InGaN materials to be grown at a relatively low temperature not higher than 800 °C. While the optimum growth temperature for GaN is above 1000 °C [14], meaning that the high-temperature environment used to grow the GaN epitaxial layer may cause the decomposition of InGaN QWs, especially in the growth process of the p-type (Al)GaN cladding layer, which needs to be grown at a higher temperature to improve the doping concentration and reduce contact resistivity [15,16].

Therefore, it is necessary to investigate the decomposition behavior and internal structural change of In-rich InGaN MQWs caused by high-temperature treatment [17,18].

Some studies [18–20] have reported investigations on the internal mechanisms of thermal degradation of In-rich InGaN QWs and demonstrated that the thermal budget is the direct cause of InGaN decomposition. Recently, Julita et al. [21] reported that the diffusion of metal vacancies plays an important role in the thermal decomposition of InGaN. It is generally believed that high-temperature treatment of InGaN may lead to the formation of In clusters [22,23]. By removing the In clusters through hydrogen treatment [24] or thermal annealing [25,26] after the growth of QWs, the luminescence performance of MQWs can be improved. Recently, Hou et al. [26] reported that the interface morphology of InGaN/GaN MQWs can be improved by thermal annealing treatment on InGaN QWs. However, the heat-treatment methods mentioned above are mostly applied in the growth process of MQWs and there are few reports on the effects of heat treatment in situ on the as-grown MQWs, where the luminescence properties would also be different.

In this work, the luminescence characteristics and internal variation mechanism of InGaN/GaN MQWs at different processing temperatures were studied by simulating the temperature conditions of a p-type cladding layer growth used in the LED device preparation. Three InGaN/GaN MQWs samples were epitaxially grown via MOCVD with the same conditions, but heat treated at different temperatures after the growth of MQWs. In the heat-treatment process, we set up two temperature steps to simulate the actual growth temperatures of the p-type GaN cladding layer and Ohmic-contact layer in a GaN-based LED structure. It is found that the effect of localized states in the QWs is strengthened when the heat-treatment temperature is 880 °C and the luminescence performance is significantly improved. However, due to the higher defect density caused by the decomposition of the InGaN QW layer, the luminescence efficiency decreases when treated at a higher temperature of 1020 °C. In addition, the surface morphology of the heat-treated samples is also analyzed by atomic force microscope (AFM).

2. Experiment

Three GaN-based samples, named as samples NT, LT, and HT were prepared by metal-organic vapor deposition (MOCVD) with a two-step growth technology [27]. In which, trimethylgallium (TMGa), trimethylindium (TMIn), and ammonia (NH_3) were used as precursors for Ga, In, and N, respectively, and N_2 was employed as a carrier gas to grow GaN and InGaN layers. Firstly, a low-temperature GaN buffer layer was grown on a c-axis sapphire substrate, and then the growth temperature was raised to 1020 °C to deposit an unintentionally-doped-GaN (u-GaN) epilayer, followed by two period InGaN/GaN MQW layers with a growth temperature of 750 °C for both InGaN QWs and GaN QBs. The above-mentioned growth conditions were the same for all three samples. Then, different temperature treatments in a N_2 atmosphere were applied to the three samples and the related information is shown in Table 1. Sample NT is the as-grown sample without any subsequent heat treatment. The heat-treatment time and temperature of sample HT was 230 s at 1020 °C and followed by 120 s at 950 °C, which were chosen to simulate the optimal conditions for the growth of p-type layers and subsequent ohmic-contact layer during the actual growth process of the LED device. Additionally, in sample LT, the heat-treatment conditions were 230 s at 880 °C and then 120 s at 880 °C. Here, the relatively low heat-treatment temperature of 880 °C was chosen to be the same as the annealing temperature which we usually used in the MQW growth process.

Table 1. Growth conditions and structural parameters of three samples determined by HRXRD measurements.

Samples	Heat Treatment Temperature/Time	Well Layer Thickness (nm)	In Content of QW
NT	None	2.69	11.28%
LT	880 °C/230 s + 880 °C/120 s	2.02	11.90%
HT	1020 °C/230 s + 950 °C/120 s	4.70	5.60%

We used high-resolution X-ray diffraction (HRXRD, Rigaku SmartLab 3KW, Tokyo, Japan) and atomic force microscopy (AFM, Bruke, Bremen, Germany) to study the structural characteristics and surface morphology of the samples. Furthermore, the temperature-dependent photoluminescence (TDPL) was measured from 30 to 300 K, using a 405 nm semiconductor laser or 325 nm He-Cd laser, as excitation sources.

3. Results and Discussion

Figure 1 shows the normalized PL spectra of three samples measured at 30 K. The fluctuations observed in the spectra are caused by Fabry–Perot interference fringes. After Gaussian fitting, the luminescence peak wavelength of the samples NT, LT, and HT can be obtained as (478.1 ± 0.2), (460.0 ± 0.1), and (460.1 ± 0.1) nm, corresponding to the peak energy at 2.60, 2.70, and 2.69 eV, respectively. It displays an obvious blue shift occurring after heat-treatments. It has been reported that an elevated temperature will cause the decomposition of InGaN/GaN MQW structure [17,18,28], and maybe we could attribute the blue shift to the variation in the energy gap caused by the decline in In content. Further, a study on the internal structural change was carried out to verify the above conjecture.

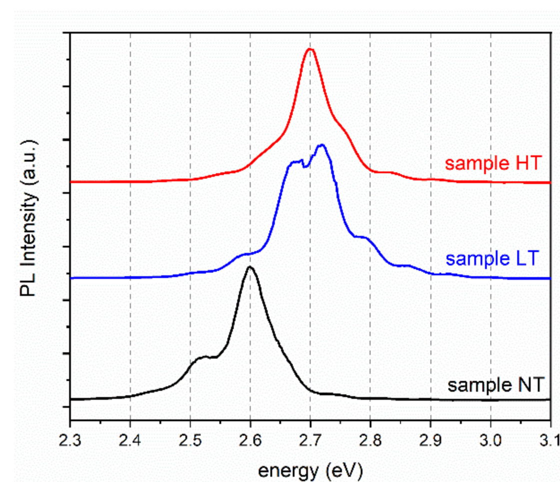

Figure 1. The normalized PL spectra of three samples NT, LT, and HT measured at 30 K.

HRXRD ω-2θ scanning curves of three samples were measured to check the indium content and well thickness of InGaN QWs. The detailed values are listed in Table 1. As shown in Figure 2, there are two main diffraction peaks in the scanning curves. The diffraction peaks located at about 34.5° originate from GaN and the peaks on the low-angle side are derived from InGaN. By fitting experimental data with the Global Fit program, as shown by the chromatic lines in Figure 2, the In content of InGaN layers can be obtained as 11.28%, 11.90%, 5.60%, respectively, for the three samples. This value decreases largely in sample HT compared with sample NT, which is the main reason for the blue shift of the luminescence peak energy in sample HT. In addition, the XRD satellite peak is less obvious in sample HT than in sample NT, meaning that the interface fluctuation becomes more serious with the increase in annealing temperature. While there is no significant difference in In concentration between sample LT and sample NT, indicating that the decrease in In content in InGaN QWs is not the reason for the blue shift when a relatively low processing temperature is used. It can be seen from the XRD results that the well thickness of sample LT decreases from 2.69 nm of sample NT to 2.02 nm. The decrease in well thickness results in an enhancement of quantum confinement effect and a decrease in quantum confinement Stark effect (QCSE), both of which cause the emission wavelength to shift to the longer wavelength direction. It has been reported that the effect of indium segregation occurs during the growth of InGaN by metalorganic chemical vapor deposition [22,29,30]. The quantum dot-like In-rich regions formed by In segregation are called In clusters, which can

serve as radiative recombination centers [22]. However, so far, the formation of In clusters in sample LT is still our speculation and will be further discussed using TDPL measurement.

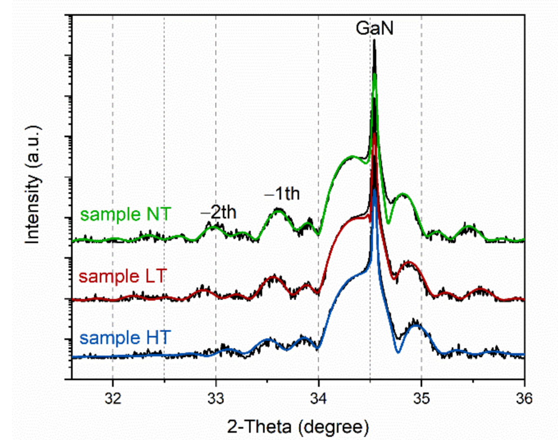

Figure 2. High-resolution X-ray diffraction (HRXRD) ω-2θ scanning curves on (0002) of three samples. The black and chromatic lines are the measurement data and fitting data, respectively. The sharpest peaks at ~34.5° in the figure come from GaN diffraction.

To further verify the model of Indium motion and structural change mentioned above, PL spectra were measured as a function of temperature ranging from 30 to 300 K using a 325 nm He-Cd laser. The peak energy and FWHM which are changing with temperature are shown in Figure 3. The luminescence peak energy shows an obvious red shift with temperature increase in three samples. To quantitatively analyze the redistribution of carriers in localization centers, a localized-states ensemble (LSE) model, which is proposed by Q. Li et al. [31] and is applicable to the full temperature range [32,33], is applied to analyze the peak energy of samples. The variation in peak position as a function of temperature from LSE is described as:

$$E(T) = E_0 - \frac{\alpha T^2}{\theta + T} - x \times k_B T \tag{1}$$

In which E_0 is the band-gap energy at 0 K. The second term is related to the temperature-induced band-gap shrinkage, α is the Varshni parameter, and θ is the Debye temperature of the material. The third term is attributed to the carriers' thermal redistribution within the localized states, in which k_B is the Boltzmann constant and x is a dimensionless parameter that can be obtained by solving the following equation:

$$x \times e^x = \left[\left(\frac{\sigma}{k_B T} \right)^2 - x \right] \left(\frac{\tau_r}{\tau_{tr}} \right) e^{(E_0 - E_a)/k_B T} \tag{2}$$

In which σ is the standard deviation of the localized distribution. $1/\tau_r$ and $1/\tau_{tr}$ are the radiative rate and escape rate of carriers, respectively, and can be taken as constant. τ_r/τ_{tr} represents the escape rate of carriers from the localization center. E_0 is the central energy of the localization center and E_a gives the occupied level of excitons at 0 K, which is similar to the Fermi level in the Fermi–Dirac distribution [34]. By fitting the peak energy with the LSE model, as shown in Figure 3a,c,e, the parameters can be obtained and are listed in Table 2. It is found that the parameter τ_r/τ_{tr} of samples LT and HT are significantly decreased compared with the untreated sample NT, indicating that the escape rates of carriers in MQWs are decreased in the heat-treated samples. Meanwhile, the standard deviation of the localized distributions is bigger in samples LT and HT, which also means that the carriers have more difficulty escaping from the localization centers and transfer among different energy levels. The LSE fitting results show that there are obvious localized

states forming in the MQWs after heat-treatment, which may be caused by the formation of more In clusters [35] or random fluctuations in quantum well thickness [36], according to XRD results.

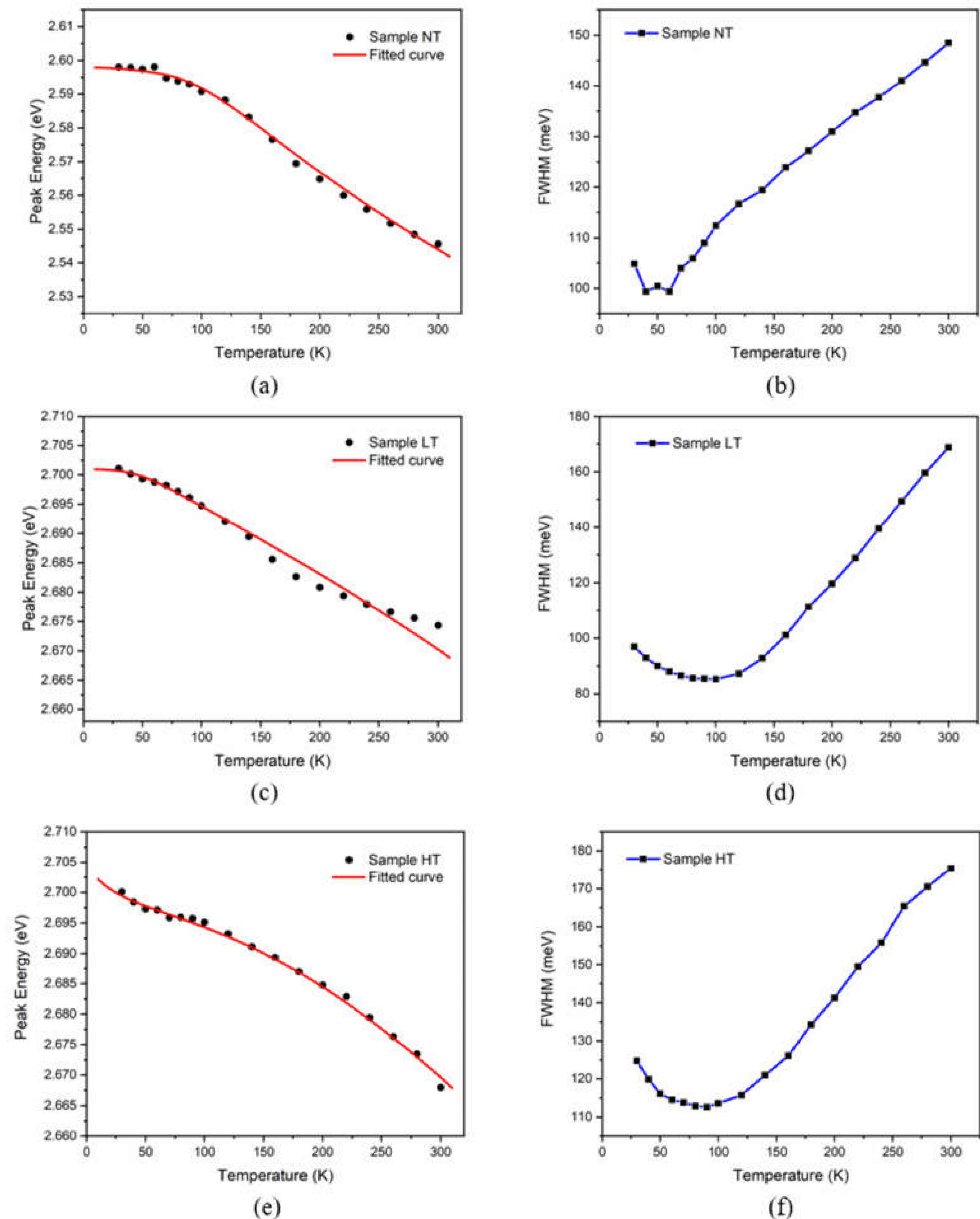

Figure 3. Peak energy and FWHM as a function of temperature obtained from temperature-dependent photoluminescence (TDPL) spectra of: (**a**,**b**) sample NT, (**c**,**d**) sample LT, and (**e**,**f**) sample HT. The symbols represent the experimental data and red solid lines in (**a**,**c**,**e**) are fitting curves using the LSE model. The blue solid lines in (**b**,**d**,**f**) show the trend of FWHM with temperature.

Table 2. Fitting parameters in the LSE model of three samples.

Samples	E_0 (eV)	E_A (eV)	τ_r/τ_{tr}	σ (meV)
NT	2.599	2.663	35	0.033
LT	2.702	2.727	0.148	0.071
HT	2.705	2.707	0.074	0.040

The FWHM shows a characteristic increase with temperature in sample NT, which is due to the increase in the interaction between photon and phonon with temperature

increasing, resulting in non-uniform Gaussian broadening. While in sample LT and sample HT, the temperature dependence of the PL peak FWHM is "V-shaped" with a critical temperature at about 100 K, as shown in Figure 3d,f. This phenomenon may be attributed to the formation of a large number of localized states in InGaN/GaN quantum wells caused by the high-temperature treatment [37]. Photogenerated carriers may be fixed in localized states with different potential well depths at an extremely low temperature and recombine radiatively. With temperature increasing, the thermal energy of excited carries increases and they tend to climb over low barriers and relax into deeper localized states, which may lead to a more concentrated distribution of carriers and a narrower spectral width. However, as the temperature rises further, the carriers gain much more energy to overcome the bound of deep localized states and jump to higher energy states; thus, broadening the spectra.

The room-temperature photoluminescence spectra of three samples were measured at the same laser power and the same optical path conditions, as shown in Figure 4. It is obvious that sample LT has the highest luminescence intensity at room temperature, which may be due to the restriction effect of the localized states on the carriers. Although the heat treatment causes more defects in the crystal, the existence of localized states makes it difficult for carriers to be captured by defects.

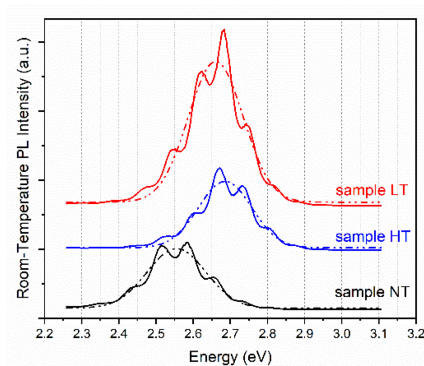

Figure 4. PL spectra (solid lines) of three samples measured at room temperature and the dashed lines show the Gaussian fitting curves corresponding to each sample. The fluctuations in the spectra are caused by the Fabry–Perot interference effect.

To further investigate the luminescence property, the normalized PL integral intensity as a function of temperature of three samples were measured by a 405 nm semiconductor laser excitation in order to avoid light absorption of GaN layers, but in all of the other sections of this article, a 325 nm He-Cd laser was used for PL measurements. In Figure 5a, we can see that when temperature is lower than 100 K, the PL intensity of samples LT and HT are almost the same and slightly higher than that of sample NT. It can be interpreted that the existence of localized states reduces nonradiative recombination at a relatively low temperature. However, as the temperature continues to increase, photo-generated carriers with higher thermal energy are more likely to be captured by defects during the process when they jump to the higher energy states and the luminescence intensity is reduced. The PL intensity of sample LT is always the highest among the three samples, and it is one order of magnitude higher than that of sample NT at 300 K, which indicates that the localized states generated by In clustering can effectively reduce the probability of carriers to be captured by nonradiative recombination centers and then improve the luminescence efficiency. However, in sample HT, which is also a sample with more localized states, there is no obvious improvement in luminescence intensity and the intensity declines with increasing temperature even faster than sample NT over 200 K. It can be inferred that the InGaN/GaN MQWs treated at 1020 °C contains more defects due to the serious structural decomposition, which increases the probability of carriers being captured by nonradiative recombination centers. It should be noted that the luminescence intensity of

both sample NT and sample HT is small at 300 K. Therefore, there is not much difference in luminescence intensity between the two samples when the electrons from GaN barrier layer are excited and luminesce, as shown in Figure 4.

The PL dependencies of normalized PL intensity of three samples were fitted by Arrhenius equation:

$$I = \frac{1}{1 + a \times \exp\left(-\frac{E}{k_0 T}\right)} \quad (3)$$

In which $I = I_T / I_{30\mathrm{K}}$, and it is the normalized integral intensity at each temperature. Parameter a is positively correlated with the number of defects. Parameter E is the activation energy of the nonradiative recombination centers. The fitting curves and fitting parameters are shown in Figure 5b and Table 3. The obtained activation energy of three samples are 41.8, 75.5, and 74.9 meV, respectively. It increases in samples with high-temperature treatment, which means that deeper potential wells were generated in samples LT and HT. Additionally, the fitting results are consistent with the previous analysis of potential well depth. The increase in parameter a from 50.3 to 254.2 indicates that high-temperature treatment causes more defects in the crystal. Although the localized states make it difficult for carriers to be captured by defects, a large number of defects will still lead to fluorescence suppression. As can be assumed in sample HT, due to the decomposition of the InGaN QW layer, higher defect density is produced and thus the luminescence efficiency decreases.

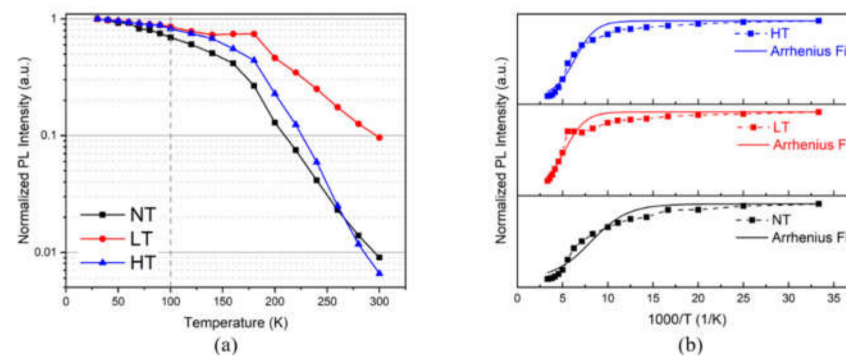

Figure 5. (**a**) Normalized PL intensity as a function of temperature of three samples. (**b**) Normalized PL intensity as a function of 1000/T and Arrhenius fitting curves.

In addition to the internal changes in the samples, we also obtained the information of surface topography. The surface morphologies of three samples were analyzed using AFM in a tapping mode, as shown in Figure 6, and the micrograph scale is $5 \times 5\ \mu m^2$. In Figure 6a, the sample NT shows a morphology of meandering steps interrupted by dislocations, while bunching steps appear in the surface of samples LT and HT, as shown in Figure 6b,c. The step width increases with the increase in heat-treatment temperature from sample NT to samples LT and HT. Additionally, it may be related to the increased migration distance of atoms at a higher temperature. The upmost GaN of samples LT and HT was decomposed and redeposited during heat treatment, which results in the atomic rearrangement and morphologic change in the surface. Meanwhile, the surface roughness increases in samples LT and HT due to trench defects caused by high-temperature treatment as can be clearly seen in AFM images. The roughness of three samples is shown in Table 4.

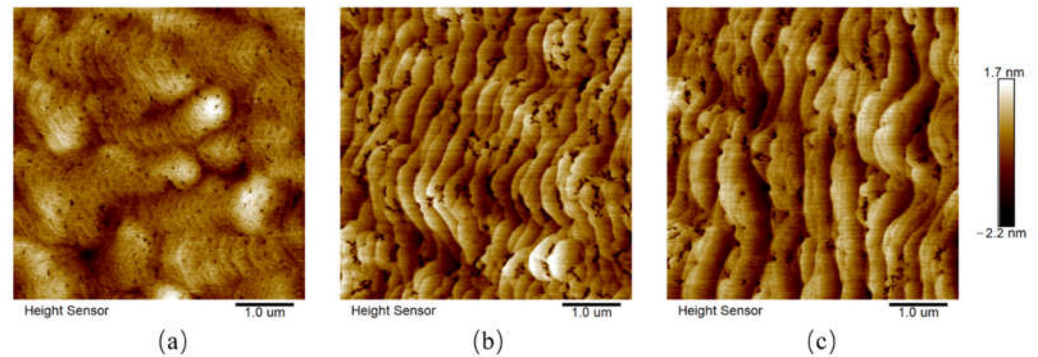

Figure 6. Surface topography measured by atomic force microscope (AFM) in tapping mode for samples of (**a**) NT; (**b**) LT; (**c**) HT.

Table 3. Arrhenius fitting parameters of three samples.

Samples	E (meV)	A
NT	41.8	50.3
LT	75.5	100.1
HT	74.9	254.2

Table 4. Roughness of three samples.

Samples	Rq (nm)	Ra (nm)
NT	0.44	0.331
LT	0.583	0.44
HT	0.568	0.454

4. Conclusions

The photoluminescence properties and surface morphology of three InGaN/GaN MQW structures heat-treated with different temperatures were investigated. We found that the formation of localized states in the QWs with decomposition of InGaN is the main reason for the improvement in luminescence characteristics of InGaN quantum wells during 880 °C heat-treatment. While the serious decomposition of the InGaN layer occurs and a large number of defect states are produced as the treated temperature rises further to 1020 °C, which causes a deterioration of luminescence performance and an increase in surface roughness. This study can provide a useful reference for the design of cladding layers and the selection of growth conditions of p-type layers during the epitaxial growth process of the device structures.

Author Contributions: Formal analysis, Y.W.; methodology, Y.W. and Y.B.; project administration, F.L. and D.Z.; writing—original draft, Y.W.; writing—review and editing, Y.B., J.Y., Z.L. and P.C. All authors have read and agreed to the published version of the manuscript.

Funding: This work was supported by the National Key R&D Program of China (Grant Nos. 2018YFB0406903), the National Natural Science Foundation of China (Grant Nos. 62034008, 62074142, 62074140, 61974162, 61904172, and 61874175), the Youth Innovation Promotion Association of Chinese Academy of Sciences (Grant No. 2019115), Beijing Nova Program (Grant No. 202093), Jiangsu Institute of Advanced Semiconductors (IASEMI 2020-CRP-02), and Young Elite Scientists Sponsorship Program by CAST.

Institutional Review Board Statement: Not applicable.

Informed Consent Statement: Not applicable.

Data Availability Statement: The data that support the findings of this study are available from the corresponding author upon reasonable request.

Conflicts of Interest: The authors declare no conflict of interest. The authors declare that they have no known competing financial interests or personal relationships that could have appeared to influence the work reported in this paper.

References

1. Buckley, E. Laser wavelength choices for pico-projector applications. *J. Disp. Technol.* **2011**, *7*, 402–406. [CrossRef]
2. Hardy, M.T.; Feezell, D.F.; DenBaars, S.P.; Nakamura, S. Group III-nitride lasers: A materials perspective. *Mater. Today* **2011**, *14*, 408–415. [CrossRef]
3. Mishia, U.K.; Parikh, P.; Wu, Y.F. AlGaN/GaN HEMTs—An overview of device operation and applications. *Proc. IEEE* **2002**, *90*, 1022–1031. [CrossRef]
4. Liang, F.; Zhao, D.; Liu, Z.; Chen, P.; Yang, J.; Duan, L.; Shi, Y.; Wang, H. GaN-based blue laser diode with 6.0 W of output power under continuous-wave operation at room temperature. *J. Semicond.* **2021**, *42*, 112801. [CrossRef]
5. Herzog, W.D.; Singh, R.; Moustakas, T.D.; Goldberg, B.B.; Ünlü, M. Photoluminescence microscopy of InGaN quantum wells. *Appl. Phys. Lett.* **1997**, *70*, 1333–1335. [CrossRef]
6. Damilano, B.; Grandjean, N.; Massies, J. InGaN/GaN quantum wells grown by molecular beam epitaxy emitting at 300 K in the whole visible spectrum. *Mater. Adv. Technol.* **2001**, *82*, 224–226. [CrossRef]
7. Wu, Z.; Shen, X.; Xiong, H.; Li, Q.; Kang, J.; Fang, Z.; Lin, F.; Yang, B.; Lin, S.; Shen, W.; et al. Improved interface quality and luminescence capability of InGaN/GaN quantum wells with Mg pretreatment. *Appl. Phys. A-Mater. Sci. Process.* **2016**, *122*, 108. [CrossRef]
8. Zhou, M.; Zhao, D.G. Barrier and well thickness designing of InGaN/GaN multiple quantum well for better performances of GaN based laser diode. *Acta Phys. Sin.* **2016**, *65*, 077802. [CrossRef]
9. Farrell, R.M.; Young, E.C.; Wu, F.; DenBaars, S.P.; Speck, J.S. Materials and growth issues for high-performance nonpolar and semipolar light-emitting devices. *Semicond. Sci. Technol.* **2012**, *27*, 024001. [CrossRef]
10. Massabuau, F.; Kappers, M.; Humphreys, C.; Oliver, R. Mechanisms preventing trench defect formation in InGaN/GaN quantum well structures using hydrogen during GaN barrier growth. *Phys. Status Solidi B-Basic Solid State Phys.* **2017**, *254*, 1600666. [CrossRef]
11. Verzellesi, G.; Saguatti, D.; Meneghini, M.; Bertazzi, F.; Goano, M.; Meneghesso, G.; Zanoni, E. Efficiency droop in InGaN/GaN blue light-emitting diodes: Physical mechanisms and remedies. *J. Appl. Phys.* **2013**, *114*, 071101. [CrossRef]
12. Huang, Y.; Wang, H.; Sun, Q.; Chen, J.; Wang, J.F.; Wang, Y.T.; Yang, H. Study on the thermal stability of InN by in-situ laser reflectance system. *J. Cryst. Growth* **2005**, *281*, 310–317. [CrossRef]
13. Karpov, S.Y. Suppression of phase separation in InGaN due to elastic strain. *MRS Internet J. Nitride Semicond. Res.* **2014**, *3*, 16. [CrossRef]
14. Liu, H.F.; Liu, W.; Yong, A.M.; Zhang, X.H.; Chua, S.J.; Chi, D.Z. Effects of annealing on structural and optical properties of InGaN/GaN multiple quantum wells at emission wavelength of 490 nm. *J. Appl. Phys.* **2011**, *110*, 063505. [CrossRef]
15. Nakamura, S.; Mukai, T.; Senoh, M.S.M.; Iwasa, N.I.N. Thermal annealing effects on P-type Mg-doped GaN films. *Jpn. J. Appl. Phys.* **1992**, *31*, L139–L142. [CrossRef]
16. Liang, F.; Yang, J.; Zhao, D.; Jiang, D.; Liu, Z.; Zhu, J.; Chen, P.; Liu, W.; Liu, S.; Xing, Y.; et al. Influence of hydrogen impurity on the resistivity of low temperature grown p-AlxGa1-xN layer ($0.08 \leq x \leq 0.104$). *Superlattices Microstruct.* **2018**, *113*, 720–725. [CrossRef]
17. Tian, A.; Liu, J.; Zhang, L.; Li, Z.; Ikeda, M.; Zhang, S.; Li, D.; Wen, P.; Zhang, F.; Cheng, Y.; et al. Green laser diodes with low threshold current density via interface engineering of InGaN/GaN quantum well active region. *Opt. Express* **2017**, *25*, 415–421. [CrossRef]
18. Li, Z.; Liu, J.; Feng, M.; Zhou, K.; Zhang, S.; Wang, H.; Li, D.; Zhang, L.; Zhao, D.; Jiang, D.; et al. Suppression of thermal degradation of InGaN/GaN quantum wells in green laser diode structures during the epitaxial growth. *Appl. Phys. Lett.* **2013**, *103*, 152109. [CrossRef]
19. Hoffmann, V.; Mogilatenko, A.; Zeimer, U.; Einfeldt, S.; Weyers, M.; Kneissl, M. In-situ observation of InGaN quantum well decomposition during growth of laser diodes. *Cryst. Res. Technol.* **2015**, *50*, 499–503. [CrossRef]
20. Liu, J.; Liang, H.; Zheng, X.; Liu, Y.; Xia, X.; Abbas, Q.; Huang, H.; Shen, R.; Luo, Y.; Du, G. Degradation mechanism of crystalline quality and luminescence in In0.42Ga0.58N/GaN double heterostructures with porous InGaN layer. *J. Phys. Chem. C* **2017**, *121*, 18095–18101. [CrossRef]
21. Smalc-Koziorowska, J.; Grzanka, E.; Lachowski, A.; Hrytsak, R.; Grabowski, M.; Grzanka, S.; Kret, S.; Czernecki, R.; Turski, H.; Marona, L.; et al. Role of metal vacancies in the mechanism of thermal degradation of InGaN quantum wells. *ACS Appl. Mater. Interfaces* **2021**, *13*, 7476–7484. [CrossRef]
22. Moon, Y.T.; Kim, D.J.; Song, K.M.; Choi, C.J.; Han, S.H.; Seong, T.Y.; Park, S.J. Effects of thermal and hydrogen treatment on indium segregation in InGaN/GaN multiple quantum wells. *J. Appl. Phys.* **2001**, *89*, 6514–6518. [CrossRef]
23. Chuo, C.C.; Lee, C.M.; Nee, T.E.; Chyi, J.I. Effects of thermal annealing on the luminescence and structural properties of high indium-content InGaN/GaN quantum wells. *Appl. Phys. Lett.* **2000**, *76*, 3902–3904. [CrossRef]
24. Hou, Y.; Liang, F.; Zhao, D.; Chen, P.; Yang, J.; Liu, Z. Role of hydrogen treatment during the material growth in improving the photoluminescence properties of InGaN/GaN multiple quantum wells. *J. Alloys Compd.* **2021**, *874*, 159851. [CrossRef]

25. Liu, S.T.; Yang, J.; Zhao, D.G.; Jiang, D.S.; Liang, F.; Chen, P.; Zhu, J.J.; Liu, Z.S.; Liu, W.; Xing, Y.; et al. The influence of thermal annealing process after GaN cap layer growth on structural and optical properties of InGaN/InGaN multi-quantum wells. *Opt. Mater.* **2018**, *86*, 460–463. [CrossRef]
26. Hou, Y.; Liang, F.; Zhao, D.; Liu, Z.; Chen, P.; Yang, J. Improvement of interface morphology and luminescence properties of InGaN/GaN multiple quantum wells by thermal annealing treatment. *Results Phys.* **2021**, *31*, 105057. [CrossRef]
27. Nakamura, S. GaN growth using GaN buffer layer. *Jpn. J. Appl. Phys.* **1991**, *30*, L1705–L1707. [CrossRef]
28. Ambacher, O.; Brandt, M.S.; Dimitrov, R.; Metzger, T.; Stutzmann, M. Thermal stability and desorption of Group III nitrides prepared by metal organic chemical vapor deposition. *J. Vac. Sci. Technol. B Microelectron. Nanometer Struct.* **1996**, *14*, 3532. [CrossRef]
29. El-Masry, N.A.; Piner, E.L.; Liu, S.X.; Bedair, S.M. Phase separation in InGaN grown by metalorganic chemical vapor deposition. *Appl. Phys. Lett.* **1998**, *72*, 40–42. [CrossRef]
30. McCluskey, M.D.; Romano, L.T.; Krusor, B.S.; Bour, D.P.; Johnson, N.M.; Brennan, S. Phase separation in InGaN/GaN multiple quantum wells. *Appl. Phys. Lett.* **1998**, *72*, 1730–1732. [CrossRef]
31. Li, Q.; Xu, S.J.; Xie, M.H.; Tong, S.Y. A model for steady-state luminescence of localized-state ensemble. *Europhys. Lett. (EPL)* **2005**, *71*, 994–1000. [CrossRef]
32. Ilahi, B.; Nasr, O.; Paquette, B.; Alouane, M.H.H.; Chauvin, N.; Saleme, B.; Sfaxi, L.; Bru-Chevalier, C.; Morris, D.; Ares, R.; et al. Thermally activated inter-dots carriers' transfer in InAs QDs with InGaAs underlying layer: Origin and dependence on the post-growth intermixing. *J. Alloys Compd.* **2016**, *656*, 132–137. [CrossRef]
33. Wang, X.; Liang, F.; Zhao, D.; Jiang, D.; Liu, Z.; Zhu, J.; Yang, J.; Wang, W. Effect of dual-temperature-grown InGaN/GaN multiple quantum wells on luminescence characteristics. *J. Alloys Compd.* **2019**, *790*, 197–202. [CrossRef]
34. Wang, Z.; Wang, L.; Xing, Y.; Yang, D.; Yu, J.; Hao, Z.; Sun, C.; Xiong, B.; Han, Y.; Wang, J.; et al. Consistency on Two Kinds of Localized Centers Examined from Temperature-Dependent and Time-Resolved Photoluminescence in InGaN/GaN Multiple Quantum Wells. *ACS Photonics* **2017**, *4*, 2078–2084. [CrossRef]
35. Cheng, Y.-C.; Lin, E.-C.; Wu, C.-M.; Yang, C.C.; Yang, J.-R. Nanostructures and carrier localization behaviors of green-luminescence InGaN/GaN quantum-well structures of various silicon-doping conditions. *Appl. Phys. Lett.* **2004**, *84*, 2506–2508. [CrossRef]
36. Grandjean, N.; Damilano, B.; Massies, J. Group-III nitride quantum heterostructures grown by molecular beam epitaxy. *J. Phys. Condens. Matter* **2001**, *13*, 6945–6960. [CrossRef]
37. Li, Q.; Xu, S.J.; Cheng, W.C.; Xie, M.H.; Tong, S.Y.; Che, C.M.; Yang, H. Thermal redistribution of localized excitons and its effect on the luminescence band in InGaN ternary alloys. *Appl. Phys. Lett.* **2001**, *79*, 1810–1812. [CrossRef]